Available online at www.sciencedirect.com
ScienceDirect
Engineering Fracture Mechanics 75 (2008) 2984–3009
Engineering Fracture Mechanics
www.elsevier.com/locate/engfracmech

Using the X-FEM method to model the dynamic propagation and arrest of cleavage cracks in ferritic steel

B. Prabel [a,b,*], S. Marie [a], A. Combescure [b]

[a] CEA, DEN/DM2S/SEMT/LISN, CE-Saclay, 91191 Gif-sur-Yvette Cedex, France
[b] LaMCoS, INSA-Lyon, CNRS UMR5259, F69621, France

Received 26 June 2007; received in revised form 26 December 2007; accepted 2 January 2008
Available online 17 January 2008

Abstract

Although initiation criteria have been the subject of many publications, the phenomena associated with the propagation and arrest of brittle cracks have not. To be able to predict the dynamic behaviour of cleavage cracks, we made a series of experiments and associated numerical studies. Tests of crack propagation and arrest were carried out on specimens of two different geometries (Compact Tension and compression ring) made of the 16MND5 ferritic steel of which French nuclear reactor vessels are constructed. The elastic-viscoplastic behaviour of this material was characterised and its nature was taken into account in the numerical simulations. The eXtended Finite Element Method (X-FEM) was developed in CAST3M finite element analysis software to enable fine, effective modelling of crack propagation. Propagation models based on principal stress were studied and it was found that critical cleavage stress depended on loading rate. The use of criteria calibrated for Compact Tension specimens gave excellent results in predictive calculations for similar specimens, and also for compression rings in both mode I and mixed-mode. The speed and path of crack predicted with the numerical simulations were in close agreement with the experimental results.

Keywords: Dynamic fracture; Crack arrest; Brittle fracture; Strain rate effects; X-FEM; Mixed-mode

1. Introduction

Ability to analyse the stability of a defect under sudden loading, as in cold thermal shock, is crucial in structure integrity analysis. It is generally assumed that it is sufficient to prove that initiation will not occur at a particular defect. Nevertheless, in order to extend the nominal service-life of some facilities, more and more elaborate safety analyses are considered. The need for plant life extension has created an incentive to improve model-based prediction. In particular, the possibility of crack arrest after its hypothetic initiation is investigated. Studies of the question have been begun in France, notably in the context of the thesis of Bouyne

* Corresponding author. Address: CEA, DEN/DM2S/SEMT/LISN, CE-Saclay, 91191 Gif-sur-Yvette Cedex, France.
E-mail address: benoit.prabel@cea.fr (B. Prabel).

0013-7944/$ - see front matter © 2008 Elsevier Ltd. All rights reserved.
doi:10.1016/j.engfracmech.2008.01.008

Nomenclature

$(\cdot)$: time derivative operator
$()_{,i}$: space derivative operator
a: crack length
a_0: crack length after pre-cracking
a_f: crack length after arrest
$\dot{a}$: crack speed
c_R: Rayleigh wave speed
$\mathbf{D}$: Hooke matrix
$[E]$: Young modulus
F_j: singular enrichment functions
G: energy release rate
H: discontinuous enrichment function
H': heavyside function
J: rice integral
K: stress intensity factor
K_J: initiation toughness (stress intensity factor calculated from J-integral)
N: usual shape functions
$\dot{p}$: equivalent inelastic strain rate
r, θ: cylindrical coordinate
T: temperature
t: time
$\underline{u}$: displacement vector
$\dot{\underline{u}}$: velocity vector
W^{ext}: external energy
W^{def}: total strain energy
W^{ela}: elastic strain energy
W^{cin}: kinetic energy
w: normalized and truncated gaussian function
w_{G}: Gaussian function
$\underline{x}$: spatial coordinate
Δt: time increment
$\underline{\underline{\epsilon}}$ or ϵ_{ij}: Green Lagrange strain tensor
$\underline{\underline{\epsilon}}^{\text{e}}$: elastic part of the strain tensor
$\underline{\underline{\epsilon}}^{\text{in}}$: inelastic part of the strain tensor
ϵ^{tot}: equivalent total strain
$\dot{\epsilon}^{\text{tot}}$: equivalent total strain rate
ϵ^{in}: equivalent inelastic strain
$\dot{\epsilon}$: equivalent inelastic strain rate
θ_c: direction of propagation
$\underline{\underline{\sigma}}$ or σ_{ij}: second Piola Kirchhoff stress tensor
σ_I: principal stress
σ_{Ic}: critical cleavage stress
σ_{Y}: yield stress
$\sigma_{\theta\theta}$: circonferential stress
σ^{stat}: static equivalent Von Mises stress (when $\dot{\epsilon}$ negligible)
σ^{eq}: equivalent Von Mises stress
Φ: yield function

ϕ:	level set function representing the crack plane
ψ:	level set function representing the crack front

[1] and Hajjaj [2]. The purpose of this paper is to propose a test-validated method of simulation for predicting the propagation of cracks under such conditions.

The technical rules and codes [3] used in nuclear design generally include provision for a crack arrest criterion, but the existing methodology is based on a static approach which, although conservative, is debatable. Many authors (such as Kalthoff and Shockey [4], Kalthoff [5] and Hahn et al. [6]) have demonstrated that a dynamic approach makes it easier to grasp the phenomena involved in unstable cleavage crack propagation. Brittleness of the material frequently results in elastic representation of it, and elastodynamic modelling of brittle fracture is frequently employed as it offers a method of analysis that is both simple and accurate [7]. Empirical relationships, based on experiment findings, link dynamic stress intensity factor K^{dyn} to the rate of propagation [8,9].

However, as emphasized by Kanninen et al. in [10], the limits of this behaviour hypothesis are not well established. Use of a more sophisticated model of the parent metal, such as an elastic-viscoplastic one, raises difficulties in defining a suitable cracking parameter and performing the numerical calculation [11].

Many crack propagation criteria can be found in the literature. These include energy criteria corresponding to general application of Griffith's approach [12], which are well defined in elastodynamic terms [13] but do not apply when the material exhibits non-linear behaviour [14]. There are also local criteria derived from initiation ones (such as the Ritchie–Knott–Rice model [15]) that appear to represent a more pragmatic approach to the problem. In recent work [2], thermal shock tests on notched rings were modelled with the help of this second type of criteria. The author considered that critical cleavage stress only depends on temperature, and that its variation mirrors that of fracture toughness. However, this was determined from the tests on the rings themselves and therefore remains debatable.

In this article a two-step methodology is used to propose, identify and validate crack propagation models. First, results of experiments on conventional specimens (compact tension) are used in numerical simulations to calibrate crack propagation criteria. Then, these calibrated criteria are used in numerical simulation to predict crack propagation (crack speed, arrest and path) for different specimens, including not only CT, but also rings specimens in both mode I and mixed-mode.

The numerical simulation is based on the eXtended Finite Element Method, developed mainly by Belytschko and Black [16], and Moës et al. [17]. This method has already been shown to be effective for solving many crack propagation problems involving three-dimensional modelling (see Moës et al. [18] and Gravouil et al. [19]) and elastodynamic modelling (see Réthoré et al. [20]), and in situations of non-linear dynamics (see Prabel et al. [21]). The crack is directly integrated into the displacement field formulation by adding specific shape functions and associated degrees of freedom. The crack is therefore not meshed explicitly, simplifying the models and also avoiding numerical problems resulting from the conventional methods of modelling crack propagation (such as node release and re-meshing, for instance).

Meanwhile, a series of experiments were made on specimens and mockups made of ferritic steel 16MND5 (A508). Cleavage of this material had already been studied in depth (see [22] and [23]). In this paper, to shed light on crack propagation and arrest, we describe tests carried out thin compact tension specimens and compression rings. Measurement of propagation was a vital aspect of the problem. The test results were examined to gain a better understanding of the phenomena involved and to define an appropriate criterion. We believe that there is a link between the rates of the phenomena involved and the loading needed for cleavage. This dependence and its consideration in crack propagation criteria is one of most important points developed in this paper.

It implies an accurate knowledge of the material behaviour at high strain rate, which can be deduced from tests on Hopkinson bars.

Beside the introduction, this paper consists of four parts.

The first describes the supporting experiments conducted. It includes characterisation of the material at high strain rate, description of the measuring instruments and the results of fracture tests.

The mechanical model and the numerical tools developed in the finite element software CAST3M [24] are described in the second part.

The third part is devoted to identification of propagation criteria, which is actually the first step of the two-step methodology adopted in this study to propose and validate models of propagation. Numerical simulation of Compact Tension specimen are performed, with crack speed imposed equal to experimental measurement.

The fourth and last part of this article focuses on the second step of the two-step methodology The criteria identified in the previous part is used in predictive numerical simulations to drive crack propagation for every specimen tested (compact tension specimens, compression rings in pure mode I and compression rings in mixed-mode). Results obtained with predictive simulations are compared to experimental measurements and validate the model of propagation proposed.

2. Supporting experiments

2.1. Description of material

The material used was 16MND5 (A508) grade ferritic steel. It was taken from a French PWR reactor vessel ring blank. Its chemical composition is given in Table 1.

Tensile tests were made at a series of temperatures between −175 °C and room temperature [25,26].

A power-type law (1) was used to describe the tensile curve of the material at any intermediate temperature,

$$\epsilon^{\text{tot}} = \begin{cases} \frac{\sigma^{\text{eq}}}{E} & \text{if } \sigma^{\text{eq}} < \sigma_{\text{Y}} \\ \frac{\sigma^{\text{eq}}}{E} + \epsilon_0 + \frac{\sigma^{\text{eq}} - \sigma'_{\text{Y}}}{E'} + \left(\frac{\sigma^{\text{eq}} - \sigma'_{\text{Y}}}{K}\right)^{\frac{1}{n}} & \text{if } \sigma^{\text{eq}} \geqslant \sigma_{\text{Y}} \end{cases} \tag{1}$$

where E, σ_{Y}, ϵ_0, E' σ'_{Y}, K, n are temperature dependent values. Their values evaluated for $T = -125$ °C are given in Table 2.

A large number of experiments were carried out with different cracked geometries to study cleavage initiation. The effects of stress triaxiality, of warm pre-stressing, and the special nature of loading of the thermal shock were carefully investigated. For the aforementioned material, ample data is available from previous work of Chapuliot et al. [25,26] and Reytier et al. [22,23]. Only the effect of strain rate remains to be determined, in order to better understand the response of the material under dynamic loading.

2.2. Dynamic characterisation of the material

High strain rate behaviour models had previously been proposed for steel of the 16MND5 type, notably by Tanguy [27] and Rossoll [28]. The latter had proposed, for instance, the Symond–Cowper [29] multiplicative law given by the following equation:

Table 1
Chemical composition of the material 16MND5 (A508)

Elements	C	S	P	Si	Mn	Ni	Cr	Mo	Cu	Co
wt%	0.16	0.005	0.006	0.19	1.35	0.74	0.18	0.51	0.07	0.01

Table 2
Values of material parameters for $T = -125$ °C

	E (MPa)	σ_{Y} (MPa)	ϵ_0	E' (MPa)	σ'_{Y} (MPa)	K (MPa)	n^{-1}
$T = -125$ °C	2.102E+5	5.520E+2	−1.169E−1	3.305E+3	1.656E+2	9.025E+2	1.190E+1

$$\sigma^{eq}(\epsilon^{in}, \dot{\epsilon}, T) = \sigma^{stat}(\epsilon^{in}, T)\left[1 + \left(\frac{\dot{\epsilon}}{D}\right)^{\frac{1}{p}}\right] \tag{2}$$

It links the dynamic equivalent stress σ^{eq} to its static value σ^{stat} via a coefficient depending on the inelastic equivalent strain rate $\dot{\epsilon}$. The coefficients derived from Rossoll's identification were: $D = 1 \cdot E8$, $p = 12$ at temperature $T = 20\,^{\circ}C$. This model has only been identified for strain rates between $10^{-3}\ s^{-1}$ and $5.5\ s^{-1}$.

To evaluate the effect of strain rate on material behaviour, tests were made on Hopkinson bars. The principle of these tests is explained in [30]. The proposed identification system is based on three strain rates (between $10^{2}\ s^{-1}$ and $10^{3}\ s^{-1}$) and seven test temperatures ($-175\,^{\circ}C$, $-150\,^{\circ}C$, $-125\,^{\circ}C$, $-100\,^{\circ}C$, $-50\,^{\circ}C$, $-25\,^{\circ}C$ and $25\,^{\circ}C$). For each possible pair, a set of tests were made. The results obtained showed greater sensitivity of the material to the temperature than to the strain rate. In particular, it was observed that plastic yielding of the material leads to adiabatic heating, and to softening of the material. Such thermal softening greatly reduces strain hardening. To better represent the effects of heating, a modified form of the Symonds–Cowper law (3) was derived:

$$\sigma^{eq}(\epsilon^{in}, \dot{\epsilon}, T) = \sigma^{stat}(\epsilon^{in}, 0, T)\left[1 + H\dot{\epsilon}^{\frac{1}{p}}\right] \tag{3}$$

where $\begin{cases} p = 4.25 - 0.015T \\ H(T, \epsilon^{in}) = a + b\exp(\epsilon^{in}/c) \end{cases}$ and $\begin{cases} a = 0.07592 - (0.07182 \cdot T/273.) \\ b = 0.06352 - (0.23970 \cdot T/273.) \\ c = 0.02528 - (0.04124 \cdot T/273.) \end{cases}$

The predictions obtained with the model were compared to the experimental results, and good agreement was found.

2.3. Fracture tests

A number of geometries have been considered for studying dynamic crack propagation, including specimens similar to the ASTM E1820 [31] CT25 type but with a thickness reduced to 5 or 10 mm to ensure uniform propagation through the thickness of the specimen, and cracked compression rings, some of which were suitable for mixed-mode initiation and propagation.

2.3.1. Description of the crack advance measuring system

All the fracture tests were made at $-125\,^{\circ}C$ to ensure all cracking would be initiated by cleavage. It is to be noted that the reference temperature determining the master curve for this material is $-120.5\,^{\circ}C$. The

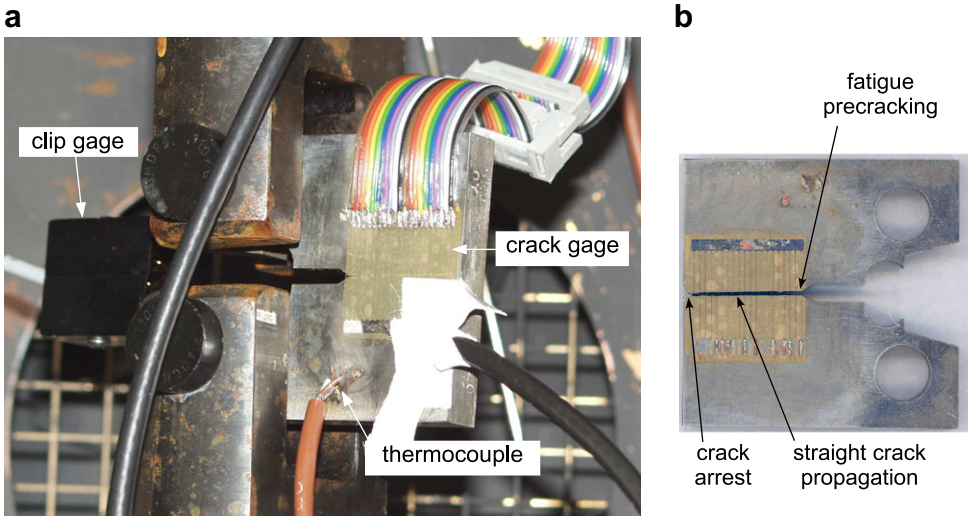

Fig. 1. (a) Experimental device for a CT specimen. (b) Straight crack path observed for ct10oy.

specimens were placed in a closed chamber in which the temperature was controlled by introducing liquid nitrogen. Under these conditions, it was not possible to use a high-speed camera or any other means of direct optical observation due to frosting. The apparatus is shown in Fig. 1.

Crack advance was measured with filament gauges along its path. As the filaments broke, the overall resistance of the gauge increased and the potential difference reading increased by stages. This signal was recorded in relation to time using a computer equipped with fast acquisition cards clocked at 60 MHz. This guaranteed adequate time resolution. One of the measurement channels was used to trigger acquisition. This signal made it possible to monitor crack growth as a function of time.

Gauges giving signals with the lowest noise were chosen. Measurement quality was verified by analysing the correlation between the crack speed signals of a pair of gauges, one on each side of the specimen. A lag of a few microseconds was sometimes observed in the case of rings. This was due to a larger thickness (25 mm) compared to the propagation length (about 7 mm). This point is covered in Section 2.3.3.

2.3.2. Description of tests on compact tension specimens

These specimens were pre-cracked under fatigue using the conventional decreasing ΔK procedure [31]. Here, we describe the compact tension specimens, whose crack path was in the plane of symmetry of the specimen. The initial and final lengths in the tests performed are given in Table 3. It also gives the initiation toughness values. The scatter observed is ordinary for cleavage crack initiation in this steel (e.g. in [22]).

Fig. 2 shows the crack speed found for compact tension specimens with a single straight crack. We notice that the higher the initiation toughness is, the faster the crack propagates. This fact reveals that the crack speed is an increasing function of the energy stored in the specimen and available to cleave. A similar trend was also reported by Kalthoff [5] and by Zehnder and Rosakis [9].

Table 3
Experimental conditions for CT specimen

Specimen		Crack length (mm)		Initiation condition	
Name	Thickness B (mm)	After pre-cracking a_0 (mm)	After crack arrest a_f (mm)	Ultimate load F_u (kN)	Toughness K_J(MPa m$^{0.5}$)
ct10oy	10	25.2	48.5	9.0	40.0
ct10oz	10	24.8	48.5	11.6	50.4
ct5pm	5	24.2	48.5	6.1	51.1
ct5pj	5	24.7	49.5	8.6	76.0

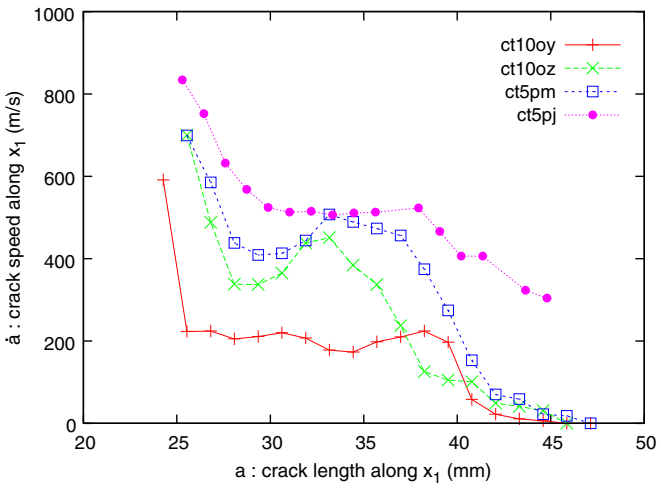

Fig. 2. Crack speed along the x-axis with respect to the crack length in CTs with straight crack paths.

Three phases can be discerned: first an abrupt initial deceleration, followed by crack propagation at a substantially constant speed then, after around 10 mm growth, deceleration until crack propagation ends.

2.3.3. Description of tests on rings

Test on rings, which have mainly been conducted by Ecole des Mines in France and Oak Ridge National Laboratory (ORNL) in the USA, can be divided into thermal shock experiments (see Bryan et al. [32] and the thesis of Genty [33], Bouyne [1] and Hajjaj [2]) and mechanical compression isothermal experiments (Iung and Pineau [34,35]). Although the thermal shock case approximates more closely to actual situations encountered in industry, the temperature gradient must be accounted for in the criterion for crack propagation and/or arrest. Temperature is an additional variable, and makes more and more complex the difficult problem of dynamic crack propagation. This explains why isothermal tests with pure mechanical loading are preferred to start this investigation, thermal shock will be studied subsequently. Fig. 3 gives details about the geometry of these isothermal rings.

Similar to the case of compact tension specimens, a decreasing ΔK procedure was used to pre-crack the rings under decreasing loading. The initial and total lengths of the cracks in the eleven tests made are shown in Table 4.

Concerning rings in mode I, as propagation length was very short, very high resolution gauges were used, with twenty filaments over 5 or 10 mm, making it possible to monitor dynamic crack propagation accurately.

It was observed that the readings from the opposite sides of the specimen were slightly out of sync. This was assumed to be because the specimen was relatively thick (25 mm) compared to the total crack progression (about 7 mm). If cleavage initiated at a point very close to one side of the specimen, it would be detected first by the gage located on this side, and then by the gage located on the other side of the specimen. The out of sync was less than the time taken for the crack to propagate along a distance equal to the thickness of the ring, which substantiated this assumption. Although the synchronisation error was not negligible, it did not change the variation of the rate of propagation with crack length. For nearly all the specimens, the measurements of crack tip advance as a function of time were in close agreement, whatever the initial crack length and at slightly different moments of initiation.

To perform mixed-mode tests, another notch was cut in the ring to incline the plane of cracking by 25° to horizontal in the fracture test (but fatigue pre-cracking is made in pure mode I). This geometry is described in Fig. 3b.

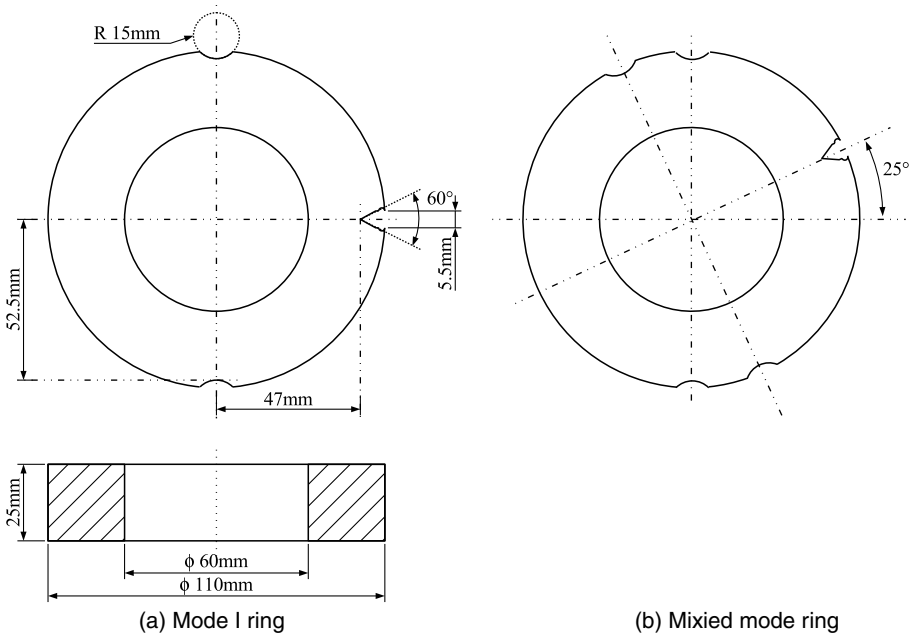

Fig. 3. Ring specimen geometry description.

Table 4
Experimental conditions for ring specimen

Specimen		Crack length (mm)		Initiation condition	
Name	Mode	After pre-cracking a_0 (mm)	After crack arrest a_f (mm)	Ultimate load F_u (kN)	Toughness K_J (MPa m$^{0.5}$)
520si	I	1.9	9.6	−201.2	55
520sh	I	2.9	9.6	−192.0	52
520un	I	0.9	9.5	−214.2	62
520um	I	2.1	8.7	−233.8	73
520uo	I	1.1	10.1	−215.7	59
520us	I	2.1	9.8	−210.5	61
520ut	I	1.4	9.0	−233.0	79
520uq	I	1.6	9.2	−219.1	66
520uv	Mixed	1.3	–	−250.7	–
520uw	Mixed	2.0	–	−271.9	–

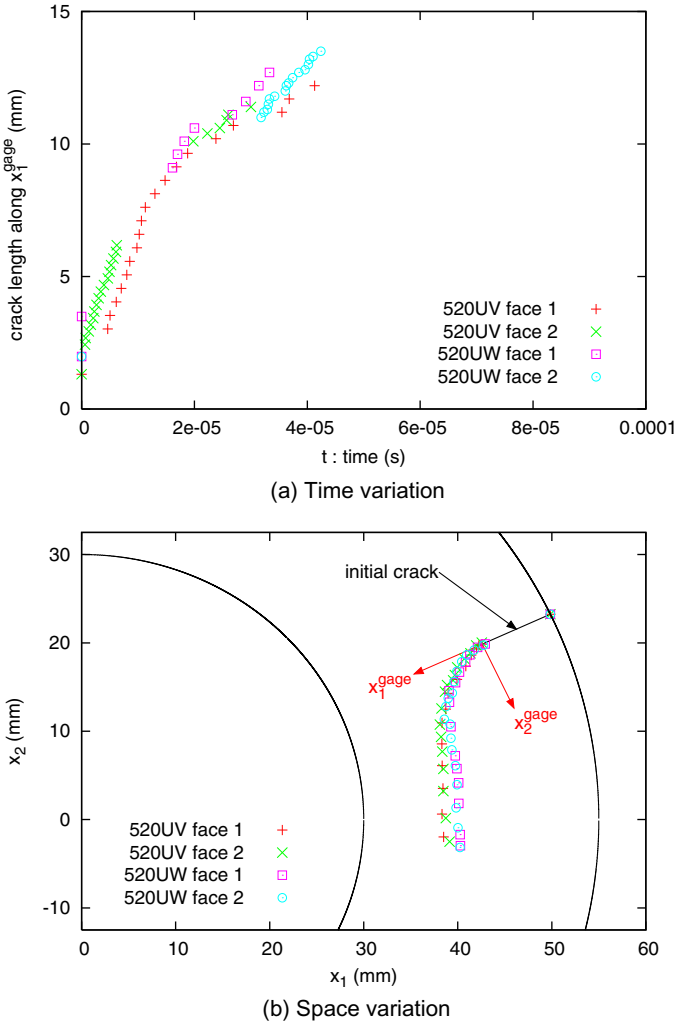

Fig. 4. Crack evolution for ring specimen in mixed-mode.

For these rings, the crack length at arrest is not given in Table 4 as crack growth was not uni-directional.

In the case of mixed-mode rings, in addition to crack front variation as a function of time (Fig. 4a), the crack path is a major result particularly interesting to assess the numerical method and model (Fig. 4b).

2.4. Fracture surface analysis

The fracture surfaces were observed with a scanning electron microscope to answer the following questions. What was the failure mode in cleavage propagation? How did the surface vary in the vicinity of the arrest front? What particularities could be observed?

Top of the Fig. 5 shows a typical fracture surface with the geographical features of cases where the crack speed is high. It can be seen that the surface is a typical cleavage fracture one. No signs of any large ductile ligament are visible.

The bottom of the Fig. 5 shows fracture surface observed for the same specimen, but in the vicinity of the crack arrest front. It indicates once again that cleavage is the only fracture mechanism involved (no large ductile ligament). Shear steps reveal that at this stage of propagation there is not enough energy available for fracture to take place in planes located at the same height. The crack tries to reach nearby planes which are the most easily dissociable, and they are not necessary located at the same height.

3. Modelling

3.1. Mechanical model

Let us consider a solid body Ω with a crack $\Gamma_+ \cup \Gamma_-$ as shown in Fig. 6.

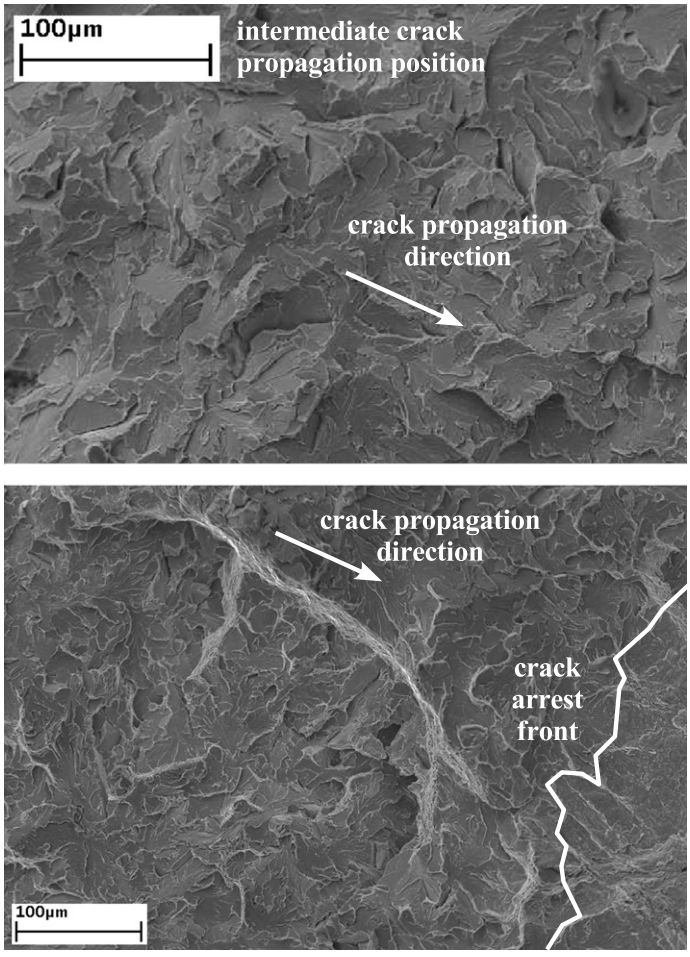

Fig. 5. Fracture surface of the ct10oy specimen at an intermediate crack propagation position (top), and at a position close to the arrest front (bottom).

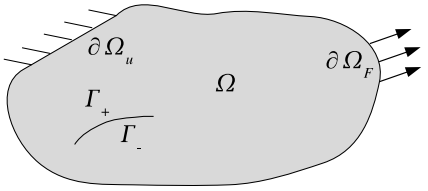

Fig. 6. Notation for the mechanical model.

Displacement of point $\underline{x}$ at instant t is written $\underline{u}(\underline{x},t)\cdot(\boxed{error}) = \partial()/\partial t$ is the time derivative operator. The fields under consideration are handled via the second Piola Kirchhoff stress tensor $\underline{\underline{\sigma}}$, and the Green Lagrange large strain tensor (4). Note that the limited displacement and strains observed in the specimen (from both experimental and numerical standpoints) would have justified a simple small-perturbation hypothesis ($u_{k,i}u_{k,j} \approx 0$),

$$\epsilon_{ij} = \frac{1}{2}(u_{i,j} + u_{j,i} + u_{k,i}u_{k,j}) \tag{4}$$

The solution satisfies the dynamic equilibrium, the initial and the boundary conditions, as defined by the following equation set:

$$\underline{\mathrm{div}}(\underline{\underline{\sigma}}) = \rho\underline{\ddot{u}} \quad \text{in } \Omega \tag{5a}$$

$$\begin{cases} \underline{\underline{\sigma}}\cdot\underline{n} = \underline{F}^{\mathrm{ext}} & \text{on } \partial\Omega_F \\ \underline{\underline{\sigma}}\cdot\underline{n} = \underline{0} & \text{on } \partial\Gamma_+ \cup \Gamma_- \\ \underline{u} = \underline{u}^{\mathrm{ext}} & \text{on } \partial\Omega_u \end{cases} \tag{5b}$$

$$\begin{cases} \underline{u}(\underline{x}, t=0) = \underline{u}^0 & \text{in } \Omega \\ \dot{\underline{u}}(\underline{x}, t=0) = \dot{\underline{u}}^0 & \text{in } \Omega \end{cases} \tag{5c}$$

The elastic-viscoplastic material behaviour under isotropic strain hardening was described by the following equation set:

$$\text{Strain decomposition into elastic and inelastic part : } \underline{\underline{\epsilon}} = \underline{\underline{\epsilon}}^{\mathrm{e}} + \underline{\underline{\epsilon}}^{\mathrm{in}} \tag{6a}$$

$$\text{with } \underline{\underline{\epsilon}}^{\mathrm{e}} = \mathbf{D}^{-1}\underline{\underline{\sigma}} \tag{6b}$$

$$\text{and } \dot{\underline{\underline{\epsilon}}}^{\mathrm{in}} = \begin{cases} 0 & \text{if } \Phi\left(\underline{\underline{\sigma}}, p, \dot{p}\right) < 0 \\ \dot{p}\frac{\partial\Phi}{\partial\underline{\underline{\sigma}}} & \text{if } \Phi\left(\underline{\underline{\sigma}}, p, \dot{p}\right) = 0 \end{cases} \tag{6c}$$

where $\mathbf{D}$ is the Hooke matrix, $\Phi(\underline{\underline{\sigma}}, p, \dot{p}) = \sigma^{\mathrm{eq}} - \sigma_{\mathrm{Y}}(p, \dot{p})$ is the yield function, σ^{eq} is the equivalent Von Mises stress, and σ_y is the threshold stress.

Note that σ_{Y} depends on the strain rate via the equivalent inelastic strain rate $\dot{p}$, defined by $\dot{p} = \sqrt{\frac{2}{3}\dot{\underline{\underline{\epsilon}}}^{\mathrm{in}} : \dot{\underline{\underline{\epsilon}}}^{\mathrm{in}}}$. The constitutive law is then integrated taking care of this dependence, as it is explained in Section 3.2.2.

In all the analyses, plane strain condition was assumed. This appeared to be justified for rings with a thickness of 25 mm, but more debatable for compact tension specimens, particularly ct5pj. This was because this 5 mm thick specimen initiated relatively late and therefore exhibited higher plasticity at the crack tip than the others. The plane strain hypothesis substantially reduces the state of plasticity at the crack tip and therefore has a non-negligible effect on stress. The hypothesis was not sufficiently realistic for this specimen only. A three-dimensional calculation could have dispelled any doubt. However, we restricted our numerical developments to the two-dimensional case (see Section 3.2.1), and no further consideration was given to the issue.

In the case of compact tension specimens, the boundary conditions and their variations with time can play a non-negligible role, particularly towards the end of propagation, as already demonstrated by Kaninnen et al.

[36]. We elected to impose them via an elastic rod representing the compliance of the tensile testing machine, thus enabling opening of the specimen during crack propagation. This was not necessary in the case of modelling the tests on rings as the movement of the bearing point due to loss of rigidity of specimen remained very slight and finally introduced very little energy into the system.

3.2. Numerical methods

3.2.1. Approximation of the displacement: the eXtended Finite Element Method

There are many finite element modelling techniques available for simulating macroscopic crack propagation. For instance the "element deletion method" consists of setting the stiffness of the cracked or damaged elements to zero, which is very crude. Another example is the "node release method", which calls for prior knowledge of the crack path and is therefore not suited for mixed-mode test simulation. Both method can be improved with re-meshing techniques (mesh-refinement and adaptation), but they necessitate a field projection step that is not fully mastered and costly in terms of calculation time. This being the case, damage mechanics and the use of cohesive zone models appeared to constitute an effective approach but limited because of difficulty to adress mesh-dependency. For the sake of completeness, the boundary element method [37], the meshless method [38] and the embedded crack model [39] must be mentioned as alternatives. In this context, methods based on partition of unity [40] appear to constitute promising approaches, essentially because they eliminate the need of conformal mesh. The eXtended Finite Element, proposed notably by Belytschko and Black [16] and Moës et al. [17], has two main features.

The first is crack description. This offers freedom from the meshing of the structure as crack location is established in a totally implicit manner by a pair of level functions. Their iso-zero determine the crack plane and the crack front, as shown in Fig. 7.

Propagating a crack is a matter of updating the values of these function. Care is taken in this operation, by using the version of the Gravouil's algorithm proposed in [19] and modified by Duflot in [41] for large propagation angle. Furthermore the level set update is performed in an efficient and accurate way with the help of an auxiliary regular grid technique, which is exposed in [21].

Evolution of level set functions reflects the progression of the crack front. Information about the crack position is then used to improve approximation of the displacement field with the functions in addition to the usual finite element ones (the usual shape functions are designated here by N). These additional functions make it possible to represent:

- the discontinuity introduced by the crack (by means of the "jump" function designated H),
- the singularity at the crack tip, (by means of function F_j).

Displacement in the element is then expressed by the following relationship:

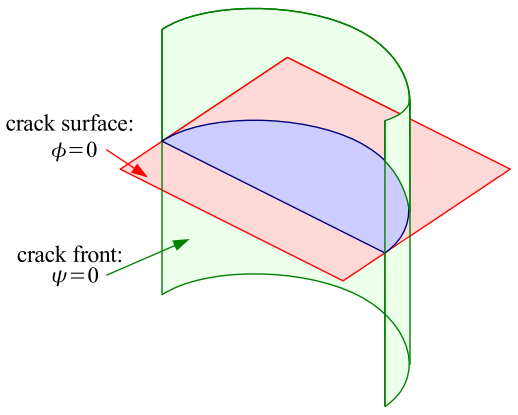

Fig. 7. Definition of the crack geometry from the level set functions ψ and ϕ.

$$\underline{u}(\underline{x}) \simeq \sum_i N_i(\underline{x})\underline{u}_i + \sum_{i\in I_H} N_i(\underline{x})H(\underline{x})\underline{a}_i + \sum_{i\in I_F} N_i(\underline{x})\left(\sum_{j=1,\ldots,4} F_j(\underline{x})\underline{b}_{i,j}\right) \tag{7}$$

where $H(\underline{x}) = \begin{cases} +1 & \text{if } \phi > 0 \\ -1 & \text{if } \phi < 0 \end{cases}$ and $F_j(\underline{x}) = \sqrt{r}\begin{cases} \sin(\theta/2) \\ \sin(\theta/2)\sin(\theta) \\ \cos(\theta/2) \\ \cos(\theta/2)\sin(\theta) \end{cases}$

Choice of functions F_j based on LEFM asymptotic solution is not prohibitive even if the material is elastic-viscoplastic, because these functions enable an approximation of the solution which is far better than the one of traditional shape functions (first or second order polynome). The choice of a basis of function calculated from the HRR solution was proposed by Elguedj et al. [42], but it should be noted that the HRR solution is no longer valid as crack propagates and unloading occurs behind the crack front. Moreover, dynamic propagation implies that solution should depend on crack speed, which complexify the problem once more.

I_H and I_F designate all the nodes belonging to an element traversed by the crack and containing the crack tip, as shown in Fig. 8.

This method is particularly well-suited for crack propagation modelling. Even though practical and theoretical effort have to be made to solve three-dimensional fracture problems (concerning for example the computation of stress intensity factors [43,44]) the application of the X-FEM remains an efficient and pragmatic numerical method, specially when complex crack path are concerned as in [19].

It even allows conservation of the energy of the numerical system under elastodynamic conditions (see Réthoré et al. [20]).

The introduction of discontinuous, non-polynomial functions means that caution must be exercised with the numerical integration of enriched elements. We therefore used a non-conforming method of sub-division described by Elguedj [42] and Prabel [21]. This enabled precise, straightforward integration of enriched elements. In addition, it avoids the projection of mechanical fields (stresses and strains) into a high-gradient zone (the crack tip). The technique of level set function updating in an auxiliary grid described in [21] is used in the mixed-mode case.

Use of the spatial approximation given by Formula (7) under the virtual power principle (8a) does not change the nature of the system to be solved (8b) relative to the classic finite element method. The only effect of enrichment is to add a few additional unknowns,

$$\int \rho \underline{v}^* \ddot{\underline{u}} + \int tr(\underline{\underline{\epsilon}}(\underline{v}^*) : \underline{\underline{\sigma}}) = \underline{v}^* F^{\text{ext}}, \forall \underline{v}^* \in V^0 \tag{8a}$$

where $V^0 = \{\underline{v}, \underline{v} = 0 \text{ on } \partial\Omega_u\}$, leads to the finite element system to be solved:

$$M\ddot{u}_{n+1} + F^{\text{int}}_{n+1} = F^{\text{ext}}_{n+1} \tag{8b}$$

The time approximation used is that proposed by Newmark [45] of average acceleration ($\gamma = 1/2, \beta = 1/4$) which is unconditionally stable, as described by the following equation:

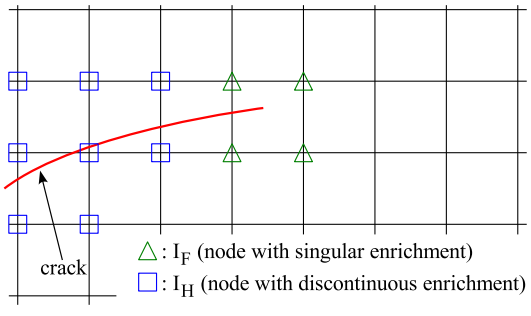

Fig. 8. Enrichment strategy.

$$\begin{cases} u_{n+1} = u_n + \Delta t \dot{u}_n + \Delta t^2 \left(\frac{1}{2} - \beta\right) \ddot{u}_n + \Delta t^2 \beta \ddot{u}_{n+1} \\ \dot{u}_{n+1} = \dot{u}_n + \Delta t (1 - \gamma) \ddot{u}_n + \Delta t \gamma \ddot{u}_{n+1} \end{cases} \tag{9}$$

Knowing the mechanical fields (displacement, stresses, strains and internal variables) at instant n, it is sought to determine the dynamic equilibrium at instant $n + 1$. The non-linear behaviour of the material results in use of an iterative system of the Newton–Raphson type to solve the problem. One key aspect of this system is the calculation of plastic flow.

3.2.2. Integration of the elastic-viscoplastic constitutive equation

Given the solution at time t and a total strain increment, it is required to calculate stresses, internal variables and inelastic strains at instant $t + \Delta t$. There are many ways available for integrating an elastic-viscoplastic constitutive law. The main one is explicit and consists in using the strain rate obtained in previous calculation step: $\dot{\epsilon}^{\text{in}} = (\epsilon_t^{\text{in}} - \epsilon_{t-\Delta t}^{\text{in}})/\Delta t$. Although this is effective in an explicit computer code, the main problem is that the method is ill-suited for the crack propagation problem. This is because the inelastic strains (and hence their variations) are located at the crack tip, which is not located at the same position in successive time steps.

The solution we adopted for calculation of the stresses depends on the implicit definition of the strain rate given by the following equation:

$$\dot{\epsilon}^{\text{in}} = \frac{\epsilon_{t+\Delta t}^{\text{in}} - \epsilon_t^{\text{in}}}{\Delta t} \tag{10}$$

The flow algorithm described by Ortiz and Simo [46] was suitable for the elastic-viscoplastic model that we chose for our work.

The algorithm features two stages: elastic prediction, followed by a radial return on the loading surface.

4. Identification of the propagation model

4.1. Choice of a local criterion

To model the propagation of a cleavage crack, two types of criteria are generally applied: energy-related and local.

Energy-related criteria are based on the concept of the energy release rate G. In the case of quasi-elastic behaviour of the structure (the small-scale yielding hypothesis), or of proportional loading without unloading, G is relatively easily assessed using integrals independent of the contour as Rice's integral J [47]. However, the use of an energy-related approach becomes much more complicated to apply in cases where it is not possible to disregard non-linearity of the behaviour of the material, effects due to the history of the loading or specific deterioration mechanisms. Freund et al. [14] and more recently Nguyen et al. [48] agree on separating the energy used up by crack growth into two terms:

- dissipation due to (visco-)plastic behaviour of the material,
- the energy absorbed in cleavage to separate the surfaces.

This separation was not directly accessible in the experiment as the plastic dissipation substantially depended on the loading conditions, the geometry and the strain rate. It was for this reason that Freund et al. [14], then Mataga et al. [49] and finally Xu and Saigal [50] sought to express the ratio between the energy used to create surfaces G^{tip} and the external energy G^{ext} as a function of crack speed $\dot{a}$. The authors considered propagation at constant speed, the $G^{\text{tip}} = G_c$ criterion, and disregarded certain terms, such as the elastic energy trapped in the plastic wake of the crack. However, it was apparent that the crack speeds predicted with this type of model were higher than the values found in experiments.

Therefore, a local stress criterion appeared to be both sound in principle and to have potential for bridging a clearer understanding of the phenomena involved and better interpreting them. In the past, the Ritchie, Knott and Rice [15] criterion has been applied, which postulates brittle fracture when the maximum principal

stress reaches a critical value at a certain distance from the crack tip. The authors sought to relate this distance to a variable that was a characteristic of the material (such as twice the grain size).

Unlike other authors (such as Bouyne [1]), we did not observe any ductile ligament on the fracture surface being the crack front. Therefore, the only mechanism involved in failure was separation of the cleavage planes. This depended on loading ahead of the crack tip, justifying the use of the RKR model.

Application of a local fracture model requires accurate knowledge of the behaviour of the material. In the case of dynamic cleavage crack propagation, viscosity may appear to be a determining factor underlying the phenomena (see [10]). Among the most recent works on the subject, that of Hajjaj [2] adopts a similar approach for the simulation of crack propagation in a ring under thermal shock. He modelled the propagation and arrest of a crack by assuming elastic-viscoplastic behaviour of the material studied (PWR reactor vessel steel). In his analysis, the author uses a RKR criterion, and supposes that the critical cleavage stress depends only on the temperature, in the same way as vary the initiation toughness with temperature.

4.2. Methodology

In this part we describe how we sought to verify the pertinence of an RKR-like criterion for governing dynamic crack propagation and propose a propagation criterion of this type. We accordingly modelled the compact tension specimen tests with straight crack lines, imposing a crack speed equal to that found in experiments.

It was also necessary to assess the impact of the numerical method used for calculating the stress with this criterion. We identified three methods for assessing the principal stress at the crack tip:

- The principal stress at a point located at a fixed distance from the crack tip in a given direction (such as $r = r_c, \theta = \theta_c$) can be interpolated. As the stress values at the Gauss points are known, their evaluation at arbitrary points suffers from numerical approximations due the interpolation method.
- It is also possible to test the principal stress value at each Gauss point.
- Finally, it is possible to average the stresses in a fixed-form zone near the crack tip.

The first method is certainly the most commonly used as it represents straightforward application of the RKR criterion: the principal stress in a direction considered critical is calculated at a point. Although the critical distance used is objective, extrapolation of the known stresses at the Gauss points to a given point in space introduces error that is all the greater if the stresses vary strongly in the region of study. Finally, to choose a length that is both close to the microstructural entity of the material and preserve a relatively good quality, we elected to consider a critical distance r_c of 100 μm.

$$\text{RKR criterion } (r_c) : \sigma_I(r = r_c, \theta = \theta_c) = \sigma_{Ic} \tag{11}$$

The second method is that used by Mariani and Perego [51], Wells and Sluys [52] and Remmers et al. [53]. To determine whether there is propagation or not, some authors compare the maximum principal stress at each of the Gauss points to elements near the crack tip to a critical value. If it is exceeded, an cohesive segment is introduced to simulate crack progression. The criterion can be met in three ways:

- at the end of each time increment without returning to the calculation of the time increment (this approach assumes a very small time increment and a sufficient number of iterations to ensure a rate of propagation that is coherent with the physics, as the process develops by discontinuous successive jumps);
- iteratively so that the criterion is precisely met at the end of each time increment.

However, the stress value at a Gauss point greatly depends on the distance between it and the crack tip. It may lead to a strong dependence of the criterion with the mesh size. Therefore, we did not test this method.

It was calculation of the propagation angle by the same authors that gave the idea of the third method of calculating the principal stress.

Mariani and Perego [51] sought, for instance, a polynomial approximation in r of the stress tensor over a half-disc at the crack tip, and they used the direction perpendicular to the maximum principal stress as the propagation direction.

Wells and Sluys [52] and Remmers et al. [53] averaged the stress tensor over a disc centred on the crack tip with a radius of three times the size of one element via Gaussian function w_G defined by (12). The idea behind these methods was not to delocalise the stress tensor (as is the case with the non-local damage models) but to avoid possible numerical errors by integrating the stresses over a small volume,

$$w_G = \frac{1}{(2\pi)^{3/2} l^3} \exp\left(\frac{-r^2}{2l^2}\right) \tag{12}$$

Instead of taking a complete disc with a radius of three times the size of one element, we opted to set dimension l over which the stress tensor was averaged. The approach thus introduced the concept of a characteristic distance as in the RKR criterion. The distance needed to be sufficiently small to characterise the state at the crack tip, but sufficiently great to define a zone of reasonable size in relation to the size of one element. We set it at 200 μm. As a Gaussian function was used to weight the average, the closer the Gauss points were to the crack tip, the more important they were. Apart from this property, the choice of the form of the weighting function remained arbitrary. It was decided not to take points where $w < 0.1$, and to normalise the stress by the integral of the weight function only. Also, as the stress state behind the crack tip did not play a predominant role in the fracture process, we only averaged the stresses over a half-disc in front of the crack front. This method of calculating the stress averaged over a half-disc can be summarised as the following set of equations:

$$\text{Half-disc criterion } (l) : \tilde{\sigma}_I \equiv \left[\frac{\int w \underline{\underline{\sigma}} \mathrm{d}\Omega}{\int w \mathrm{d}\Omega}\right]_I = \sigma_{Ic} \tag{13}$$

where $w = \begin{cases} w_0(r)H'(\psi) & \text{if } w_0 > 0.1 \\ 0 & \text{if } w_0 \leqslant 0.1 \end{cases}$, $w_0 = \exp\left(\frac{-r^2}{2l^2}\right)$, and $H'(\psi) = \begin{cases} 1 & \text{if } \psi > 0 \\ 0 & \text{if } \psi \leqslant 0 \end{cases}$ as ψ designates the level function associated with the crack front and $[\ldots]_I$ represents the maximum principal tensile stress.

4.3. Results of the compact tension specimen test, and their interpretation

A finite element calculation was made of brittle fracture of compact tension specimens by directly applying the time variation to the length of the crack as measure in an experiment. We would like to emphasise the fact that the experimental data used was raw. We simply give the results for a single specimen (ct5pm), the trends visible being the same for the other specimens.

After a quasi-static loading stage up to initiation loading (determined from toughness found in experiments), crack propagation occurred dynamically with an elastic-viscoplastic law. The energy balances

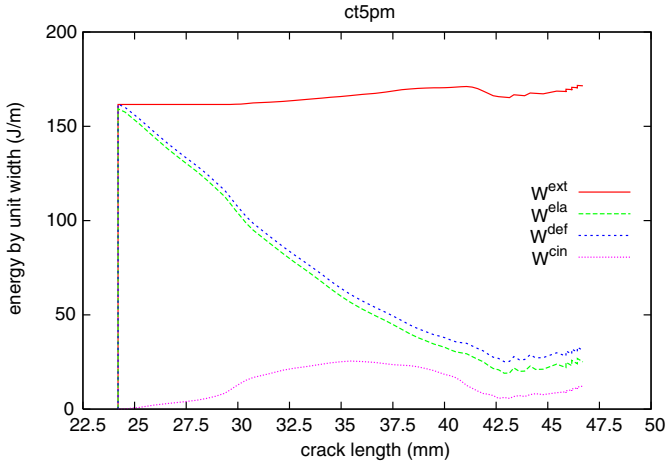

Fig. 9. Energetic term variation during propagation in specimen ct5pm.

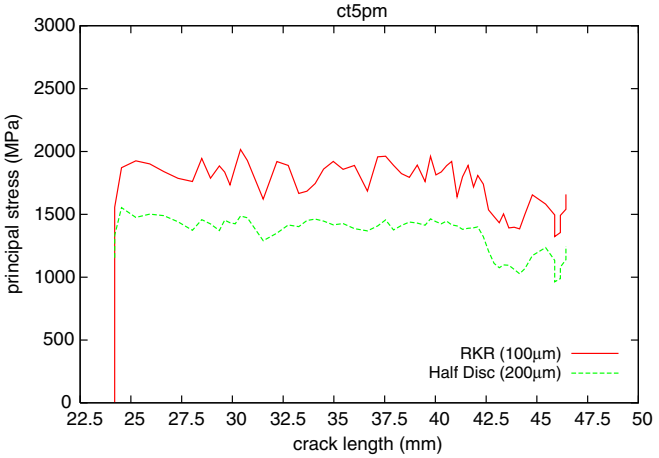

Fig. 10. Variation of measured stress in specimen ct5pm.

established on compact tension specimens (Fig. 9) show that almost all the energy stored was used to break the specimen.

The external energy W^{ext} supplied by release of the bar (which simulates the compliance of the test machine) was only negligible for the first few millimeters of propagation. The strain energies (W^{def} and W^{ela} being, respectively, the total and the elastic strain energy) decreased significantly during the propagation. The kinetic energy W^{cin} increased during half the propagation, then diminished. Similar trends have already been observed by Hahn et al. [54] in a steel double cantilever beam and by Kobayashi [55] in a polymer compact tension specimen.

For what concerns the crack tip, Fig. 10 shows the variation during propagation of the principal stress calculated with the two methods described above (RKR-method described by Eq. (11), and the average of the stress tensor on a half-disc described by Eq. (13)). The two variables vary in a similar manner. During most of the propagation, when the rate was high and nearly constant, the stress was relatively constant. As soon as the deceleration phase began (when $a > 42$ mm), the stress dropped.

To limit the scatter of the instantaneous crack speed measured in the experiments, each test was divided into time intervals. These were created to be able to consider the crack speed to be constant. As a general rule, three intervals were sufficient to properly describe the variation in experiments of crack length as a function of time. For each of the intervals, an average over time of a rate and stress pair was deduced.

The curves obtained with the RKR criteria ($r_c = 100$ μm) and mean half-disc ($l = 200$ μm) are shown in Fig. 11. As previously mentioned, one of the specimens broke late with a correspondingly high level of plasticity which is not well represented by the plane strain hypothesis. Hence, we decided to exclude it from the discussion as long as we are using bi-dimensional modelling.

A small increase in the principal stress with the crack speed was observed. It has therefore decided to identify the criterion (14) for both methods of principal stress calculation using the empirical relationship originally proposed by Kaninnen and Popelar [8] for the dependence of the dynamic stress intensity factor on the rate of propagation,

$$\sigma_{Ic}(\dot{a}) = \frac{\sigma_A}{1 - (\dot{a}/v_{\text{lim}})^m} \tag{14}$$

With the above formula, the parameters were set as follows $v_{\text{lim}} = c_R$ and $m = 1$. This gave the following characteristic values: $\sigma_A = 1500$ MPa and $\sigma_A = 1150$ MPa for the RKR criterion and the mean half-disc criterion, respectively.

The observed dependence of the critical stress on the crack speed certainly indicated sensitivity of this stress to the associated strain rate. To check, top of Fig. 12 shows the variation of the stress calculated with the RKR criterion ($l = 100$ μm) with the equivalent total strain rate calculated at the same point. It effectively confirms dependence between the critical stress and the strain rate measurement.

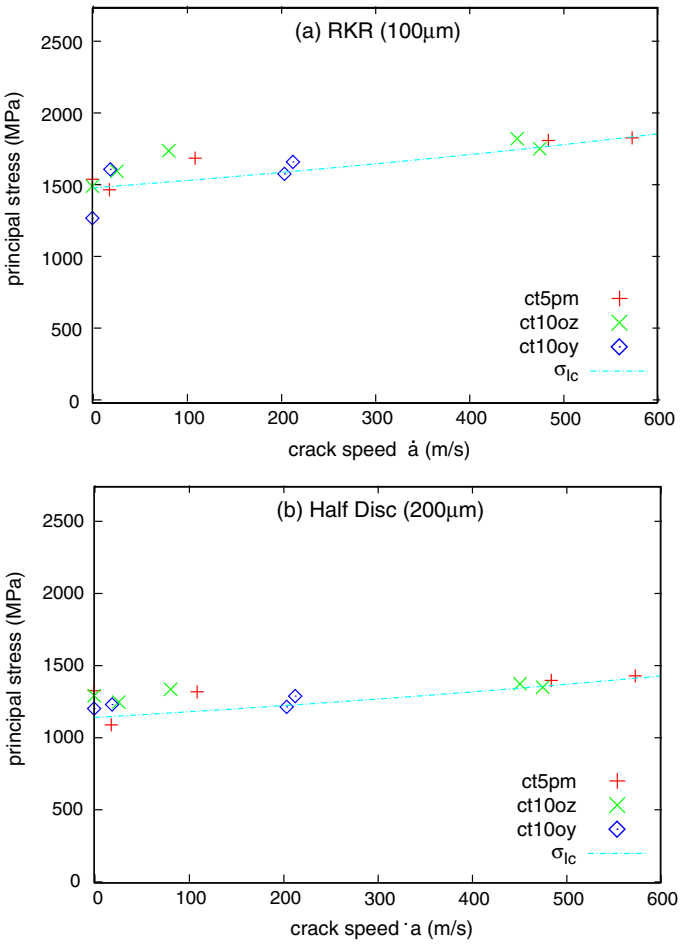

Fig. 11. Identification of criteria depending on the crack speed.

Eq. (15) shows a possible relationship between these two variables. It seems to indicate that the critical stress and the yield point exhibit a similar dependence on strain rate. However, tests at higher strain rates ($10^4\ s^{-1}$) than those made up to now are needed to substantiate this hypothesis, and possibly directly express σ_{Ic} as a function of $\sigma_y(\dot{\epsilon})$,

$$\sigma_{Ic} = \sigma_{Ic0}\left[1 + 10^{-6}(\dot{\epsilon}^{\text{tot eq}})^{1/0.63}\right] \quad \text{where } \sigma_{Ic0} \simeq 1463 \text{ MPa} \tag{15}$$

Such dependence of stress on strain rate is unusual. Constant critical stress is generally postulated in the literature. Hajjaj [2], for instance, only considered dependence on temperature for the critical stress.

An identical result was obtained with the second method of calculating the stress of a half-disc (see bottom of Fig. 12 and Eq. (16)).

Critical strain variation then takes the following form:

$$\sigma_{Ic} = \sigma_{Ic0}\left[1 + 0.1(\dot{\epsilon}^{\text{in eq}})^{1/3}\right] \quad \text{where } \sigma_{Ic0} \simeq 775 \text{ MPa} \tag{16}$$

5. Predictive modelling

To assess the relevance of the critical cleavage stress dependence we found, the two criteria proposed (critical stress as a function of crack speed and strain rate) were used to predict the results of tests on compact tension specimens and rings.

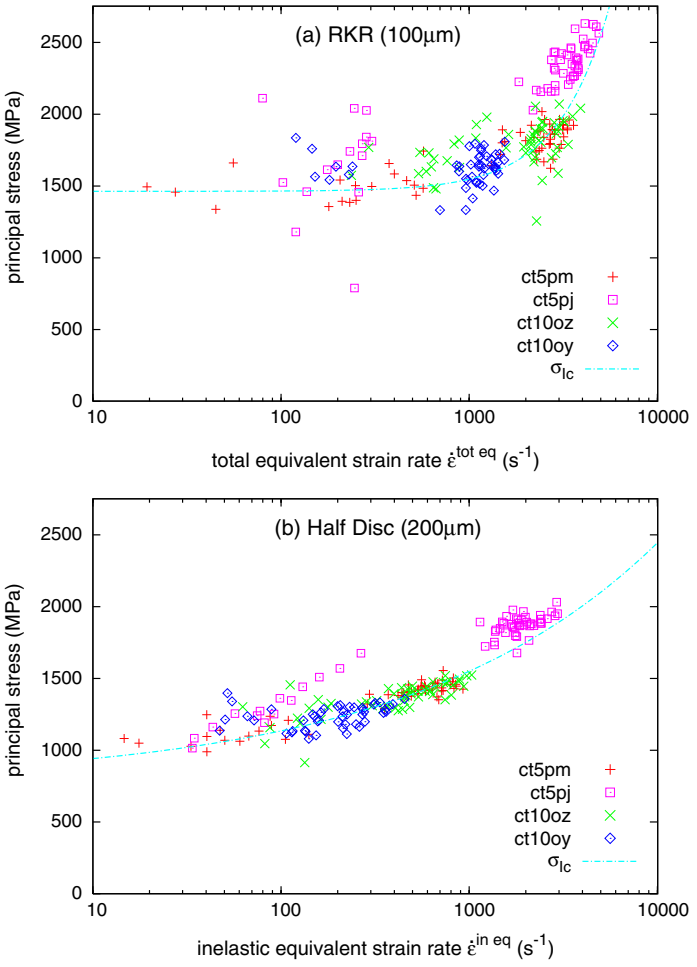

Fig. 12. Identification of a criterion depending on the strain rate.

5.1. Modelling of tests on compact tension specimens

5.1.1. Criterion dependent on crack speed

One criterion that directly uses the crack speed allows the use of an explicit algorithm for crack progression (see the following equation),

$$a_{n+1} = a_n + \dot{a}_n \Delta t \quad \text{where } \dot{a}_n = \sigma_{Ic}^{-1}(\underline{\sigma}_n) \tag{17}$$

The system can also be refined using a Runge–Kutta method, correcting the value of the crack speed to allow for the final state explicitly predicted (see the following equation),

$$\begin{aligned}
&\text{Resolution of dynamic equilibrium at time :} && t_{n+1}^{\text{try}} = t_n + \Delta t^{\text{try}} \\
&\text{Application of the criterion :} && \dot{a}_{n+1}^{\text{try}} = \sigma_{Ic}^{-1}(\underline{\sigma}_{n+1}^{\text{try}}) \\
&\text{Correction of the crack speed :} && \Delta t = \frac{\Delta a}{(\dot{a}_n + \dot{a}_{n+1}^{\text{try}})/2} \\
&\text{Resolution of dynamic equilibrium at time :} && t_{n+1} = t_n + \Delta t \\
&\text{Application of the criterion :} && \dot{a}_{n+1} = \sigma_{Ic}^{-1}(\underline{\sigma}_{n+1})
\end{aligned} \tag{18}$$

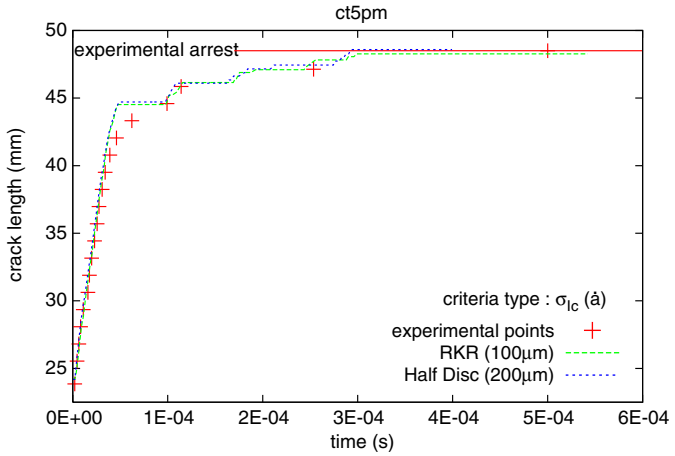

Fig. 13. Crack length variation with time for specimen ct5pm. Comparison with experiment of simulations using a critical stress depending on the crack speed.

The time increment Δt^{try} was initially set at 1×10^{-6} s, but with the possibility of being increased as the speed decreased, in order to avoid elementary advances less than the size of one element. This kept the stiffness matrix well-behaved.

Clearly, there is no particular difficulty in modelling compact tension specimens and application of this type of criterion affords excellent representation of the experimental results (see Fig. 13).

5.1.2. Criterion depending on the strain rate

Another type of algorithm needs to be considered when the criterion does not involve the crack speed, because it is implicit. For example, combining Eqs. (11) and (15) (or, respectively, Eqs. (13) and (16)) the equality to verify can take the following form:

$$B \equiv \sigma_{In+1} - \sigma_{Ic}(\dot{\epsilon}_{n+1}) = 0 \tag{19}$$

We propose the scheme described by (20). Elementary crack advance is imposed and the time increment which enables to meet the criterion is sought. If the criterion cannot be met in a time increment less than a lower limit (1E−5 for instance), the crack stops for the next time increment, and this continues until the criterion is met again,

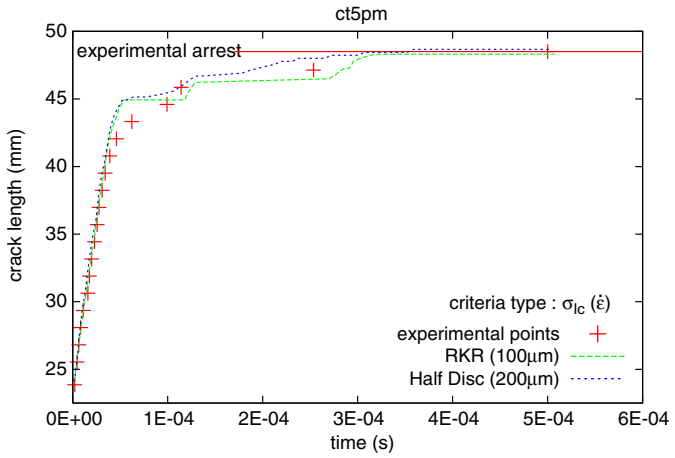

Fig. 14. Crack length variation with time for specimen ct5pm. Comparison with experiment of simulations using a critical stress depending on the strain rate.

$$
\begin{aligned}
&\text{Initialization of crack length :} && a_{n+1} - a_n = \Delta a \\
&\text{Initialization of time increment :} && \Delta t_{n+1}^{(0)} = \Delta t_n \\
&\text{Resolution of dynamic equilibrium at time :} && t_{n+1}^{(i)} = t_n + \Delta t_{n+1}^{(i)} \\
&\text{Evaluation of the criterion :} && B\left(\sigma_{In+1}^{(i)}, \dot{\epsilon}_{n+1}^{(i)}\right) \\
&\text{Correction of the crack speed :} && \Delta t_{n+1}^{(i+1)} = \Delta t_{n+1}^{(i)}\left[1 - B^{(i)}\right] \\
&\text{Iteration } i = i+1 \text{ until :} && B = 0
\end{aligned}
\tag{20}
$$

Once again, the criterion gave satisfactory result for compact tension specimens, as can be seen in Fig. 14

To confirm that the criteria were transposable, fine modelling of a ring in pure mode I and the mixed-mode was conducted.

5.2. Modelling of tests on rings

5.2.1. Pure mode I rings

Predictive simulations for rings in pure mode I were performed with the same numerical scheme and the same criteria as before. The results are shown in Fig. 15.

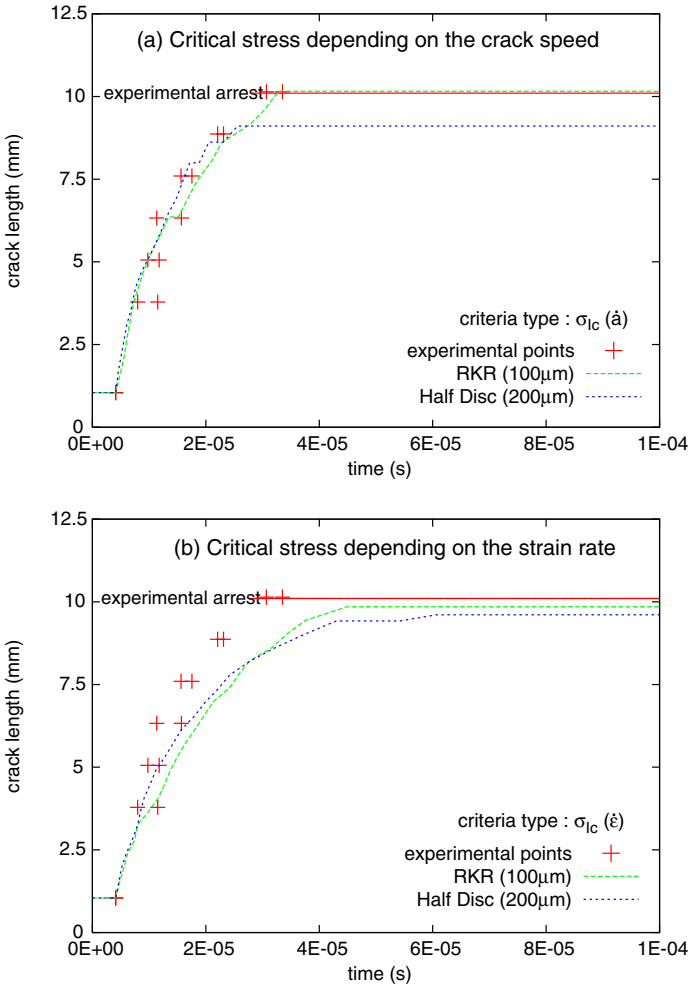

Fig. 15. Crack length variation with time in mode I ring 520uo. Comparison with experiment of simulations using a critical stress depending on the crack speed (top), and on the strain rate (bottom).

Transposition of the criteria to the pure mode I ring case gave very satisfactory results, as prediction of crack speed and crack length at arrest were very precise. This was all the more remarkable as the crack speeds and crack lengths were very different to those considered in the case of compact tension specimens, ranging from 1000 m/s in rings to a maximum of 600 m/s observed in the case of compact tension specimens.

5.2.2. Mixed-mode rings

Modelling of propagation in rings in the mixed-mode necessitates adding an additional law for predicting crack orientation to the propagation model:

– the direction of the maximum opening stress (maximum hoop stress criterion [56]),
– the direction perpendicular to the maximum principal stress field,
– the direction at which structure energy is the least (minimum of energy criterion).

The first criterion used the maximum opening stress direction. In the context of linear elastic fracture mechanics, this criterion can be readily expressed as a function of stress intensity factors,

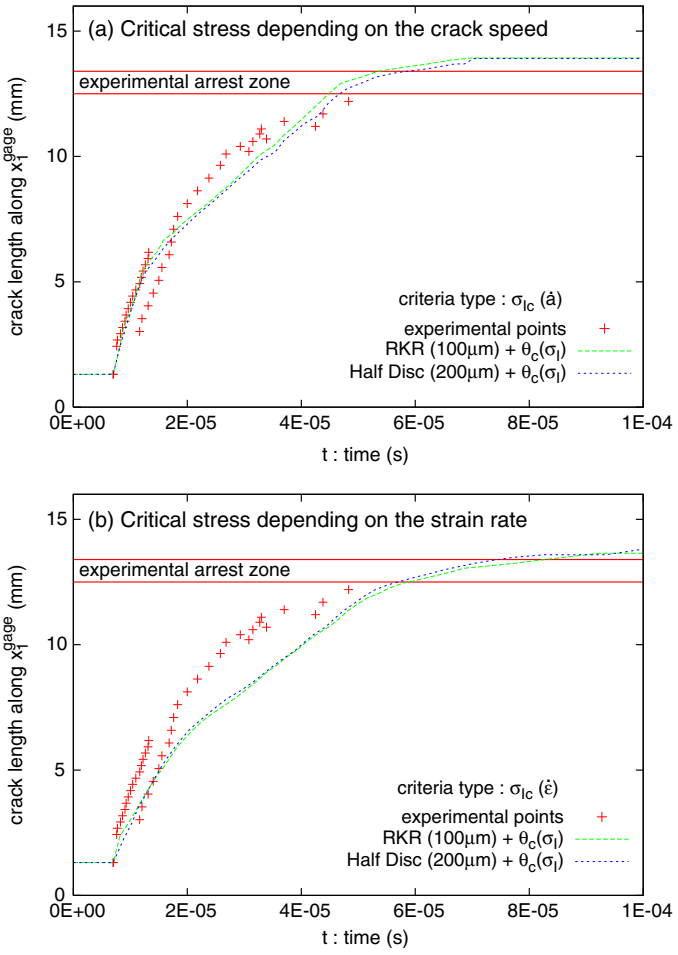

Fig. 16. Crack length variation in mixed-mode ring 520uv. Comparison with experiment of simulations using a critical stress dependent on the crack speed (top), and on the strain rate (bottom).

$$\theta_c = \{\theta, \max(\sigma_{\theta\theta})\} \tag{21a}$$

$$\theta_c = 2a \arctan\left(\frac{1}{4}\left[\frac{K_I}{K_{II}} - \text{sign}(K_{II})\sqrt{\left(\frac{K_I}{K_{II}}\right)^2 + 8}\right]\right) \text{ in LEFM} \tag{21b}$$

There are two ways of applying a criterion based on the direction perpendicular to the maximum principal stress. The first is the "global tracking algorithm" developed by Oliver and Huespe [57,58]. This method consists in calculating a function whose isovalues are perpendicular to the maximum principal stress field, and to make the crack propagate along the isovalues. The second method, which is outlined in [52], is based on a stress tensor averaged over the crack tip (average stress criterion). In Section 4.2, we gave the details concerning calculation of this averaged tensor (see Eq. (13)). The propagation direction is in this case that perpendicular to the maximum principal stress of the stress tensor.

Use of the direction that minimises the structure energy (minimum energy criterion) was, notably, studied by Dumstorff and Meschke [59] and compared to the aforementioned criteria. To ensure that our approach remained consistent, we tested criteria based on the local stresses at the crack tip.

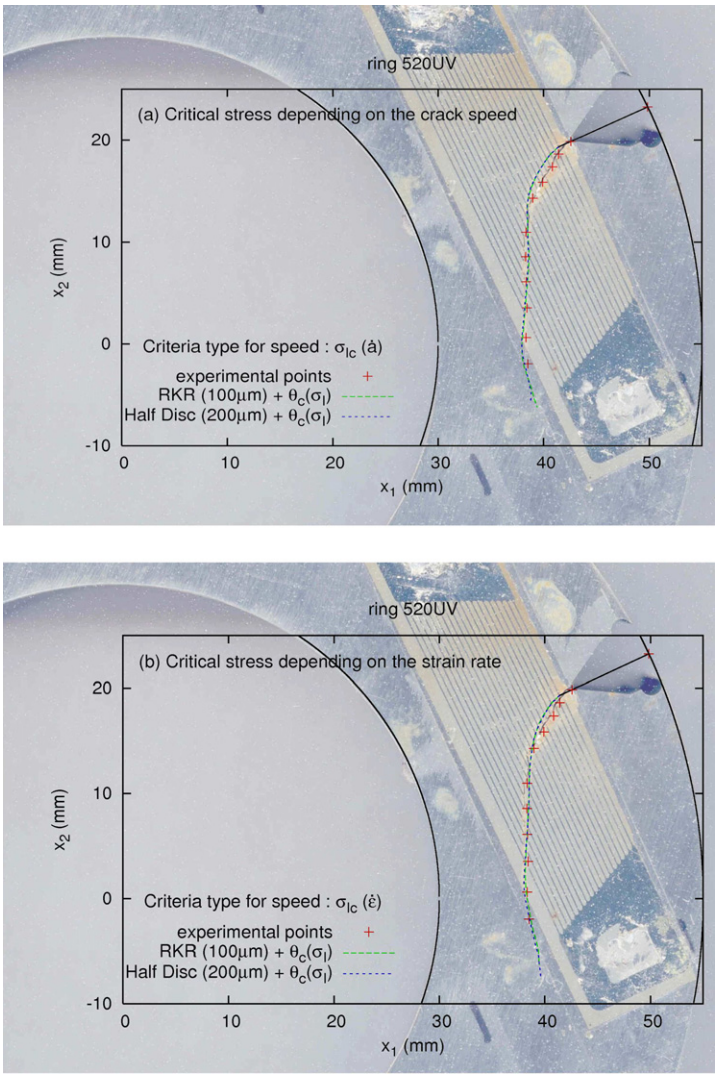

Fig. 17. Crack path variation in mixed-mode ring 520uv. Comparison with experiment of simulations using critical stress dependent on the crack speed (top), and on the strain rate (bottom).

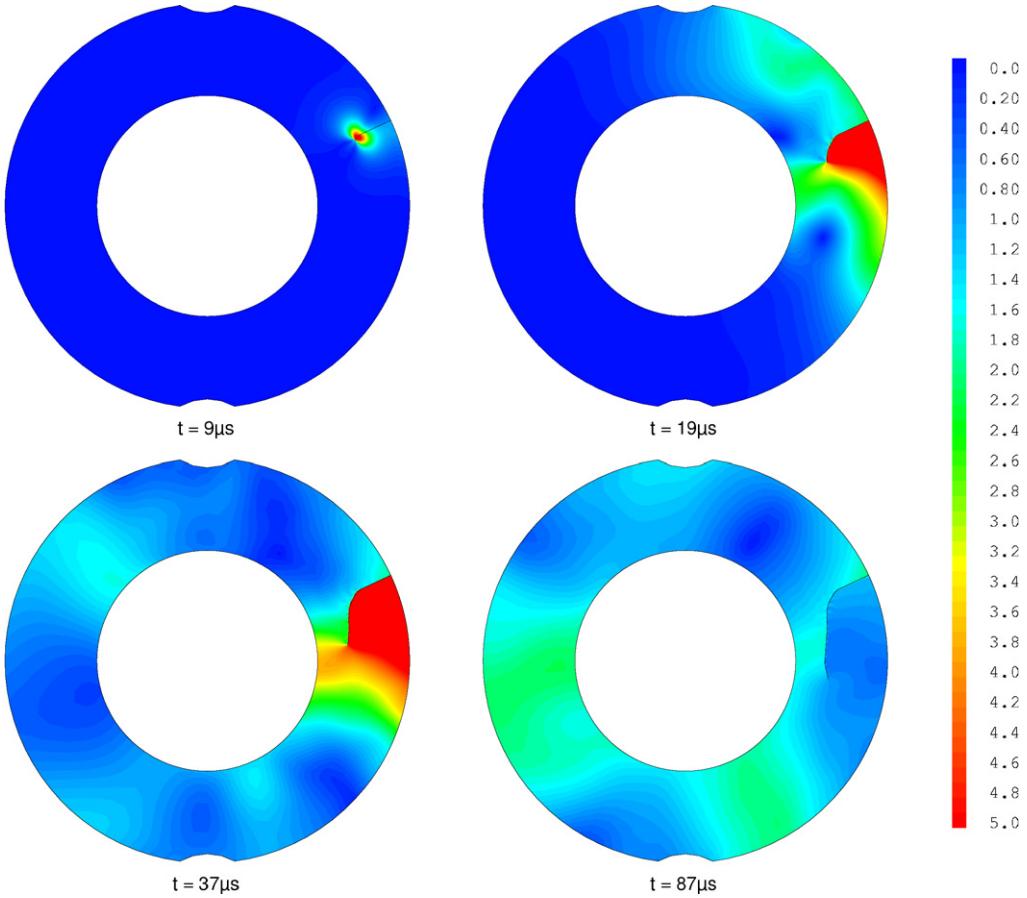

Fig. 18. Norm of the velocity $|\underline{\dot{u}}|$ (in m/s).

In principle, the maximum hoop stress criterion appears to be very close to the RKR criterion, because it evaluates opening stress [1] at a critical distance r_c from the crack tip. However, as previously mentioned, evaluation of the stress at a point (generally different from a Gauss point) is subject to numerical approximations. The results obtained with this criterion are not presented in this paper; the overall aspect of the crack path obtained is close to the physical one, but suffer from oscillations and look like sawtooth. Accordingly, we then give preference to using the average stress criterion for deciding on the critical propagation direction (designated $\theta_c(\sigma_I)$). This method gives a good crack path without any numerical oscillations.

The results of predictive simulations in terms of the crack path and variation with time are given in top of Figs. 16 and 17 and for the criteria based on a critical stress dependent on the crack speed, and in bottom of Fig. 16 and in bottom of Fig. 17 for the criteria based on a critical stress dependent on the strain rate, respectively.

The agreement was observed to be good between the experimental results and finite element simulations with both types of criterion.

A mechanical interpretation of the propagation test is proposed by plotting the norm of the velocity $|\underline{\dot{u}}|$ in Fig. 18, and the hydrostatic stress $\sigma_H \equiv Tr(\underline{\underline{\sigma}})$ in Fig. 19.

The results of these simulations enable to show how initiation triggered a mechanical wave, which could be clearly discerned in the initial instants. Then, as the crack propagated, a piece became detached from

[1] We emphasise the fact that the critical direction given by the maximum hoop stress criterion is different from the direction of the maximum principal stress. For a crack in an elastic medium under pure mode I loading, the principal stress has two maxima at angles of $+60°$ and $-60°$, whereas the hoop stress has only one maxima at $0°$ which is a more physical direction of propagation.

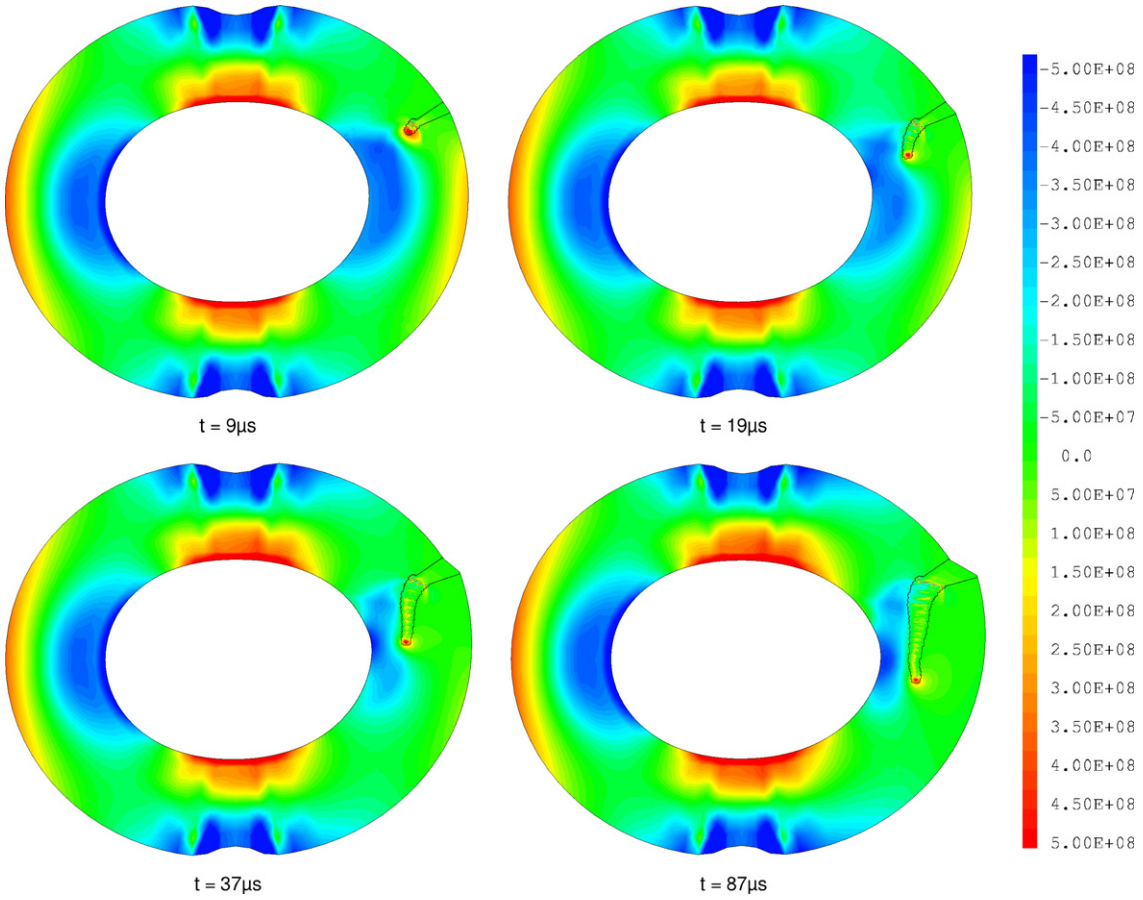

Fig. 19. Hydrostatic stress σ_H (in Pa), displacement amplified $\times 10$.

right-hand-side of the specimen, allowing the edges to separate. When the crack stopped, the piece moved to the right more slowly, stopped, then returned to the remainder of the ring, and oscillated.

The hydrostatic stress distinguished the areas under compression ($\sigma_H < 0$) from those under tension ($\sigma_H > 0$). For propagation to occur, the edges of the crack must separate. It is therefore not surprising to see that, during propagation, the crack turns to avoid the areas under compression (i.e. those on the inner surface of the ring). In reaction to the crack propagation, the right-hand-sided compression area reduces.

6. Conclusions

In order to understand the phenomena involved in the dynamic propagation and the arrest of cleavage cracks in PWR reactor vessel steel, brittle fracture tests and their modelization with the X-FEM method (an up-to-date and robust numerical tool) were performed.

Tests on different geometries enabled to determine whether the criteria proposed were transposable. We notably conducted tests on thin compact tension specimens and rings under compression, with a crack in the mode I and the mixed-mode. Scanning electron microscope examination of the crack face notably indicated the absence of ductile ligament behind the crack front during propagation, eliminating any possibility of dissipation of energy thereby. A simple stress criterion should thus make it possible to reflect propagation as, in principle, only loading of the material in front of the crack plays a role in the propagation mechanisms.

Criteria based on measurements of the principal stress at the crack tip were studied. This, in particular, showed that the critical stress depends on the crack speed and, hence, the strain rate. Relationships between

the critical stress and these variables were established and enabled prediction of the results of test on compact tension specimens and rings that was in good agreement with experiment values, particularly as concerned crack speed, crack length at arrest and crack path in the mixed-mode case.

Additional studies with a number of goals are called for. First, there is a need to verify the dependence of the critical stress on strain rate, and assess any similitude between this dependence and that known to exist between yield stress and strain rate. Then, it needs to be confirmed that the proposed criteria are transposable, on the basis of the results of other types of tests. Finally, the dependence of critical stress on temperature also needs to be covered to model the case of rings exposed to thermal shock. It would be particularly interesting to determine whether the temperature dependence were similar to that observed concerning initiation toughness or that linking yield stress and temperature.

Acknowledgements

The authors would like to thank the CEA for his financial support and Mr. Herms (CEA/DPC/SCCME) for his assistance in the fractography work.

References

[1] Bouyne E. Propagation et arrêt de fissure de clivage dans l'acier 2 1/4 Cr-1 Mo. PhD thesis, Ecole des Mines de Paris; 1999.
[2] Hajjaj M. Propagation et arrêt de fissure dans les cuves de réacteurs à eau préssurisée. PhD thesis, Ecole Centrale de Paris; 2006.
[3] Règles de Conception et de Construction relatives aux matériels Mécaniques. Annexe A16 – Tome I – Vol Z, RCC-M, AFCEN; 2002.
[4] Kalthoff JF, Shockey DA. Instability of cracks under impulse loads. J Appl Phys 1977;48:986–96.
[5] Kalthoff JF. On the measurement of dynamic fracture toughness: a review of recent work. Int J Fract 1985;27:277–98.
[6] Hahn GT, Hoagland RG, Kanninen MF, Rosenfield AR. A preliminary study of fast fracture and arrest in DCB test specimen. In: Proceedings of the conference on dynamic crack propagation, Leyden, The Netherlands; 1973. p. 649–62.
[7] Freund LB. Dynamic fracture mechanics. Cambridge University Press; 1989.
[8] Kanninen MF, Popelar CH. Advanced fracture mechanics. Oxford University Press; 1985.
[9] Zehnder AT, Rosakis AJ. Dynamic fracture initiation and propagation in 4340 steel under impact loading. Int J Fract 1990;43:271–85.
[10] Kanninen MF, Hudak SJ, Couque HR, Dexter RJ, O'Donoghue PE. Viscoplastic-dynamic crack propagation: experimental and analysis research for crack arrest applications in engineering structures. Int J Fract 1990;42:239–60.
[11] Ostlund S. On numerical modeling and fracture criteria of dynamic elastic-viscoplastic crack growth. Int J Fract 1990;44:283–99.
[12] Griffith AA. The phenomena of rupture and flow in solids. Philos Trans Roy Soc Lond 1921;221:163–98.
[13] Freund LB. Energy flux into the tip of an extending crack in an elastic solid. J Elasticity 1972;2:341–9.
[14] Freund LB, Hutchinson JW, Lam PS. Analysis of high strain rate elastic plastic crack growth. Engng Fract Mech 1986;23:119–29.
[15] Ritchie RO, Knott JF, Rice J. On therelationship between critical tensile stress and fracture stress in mild steels. J Mech Phys Solids 1973;21:395–410.
[16] Belytschko T, Black T. Elastic crack growth in finite element with minimal remeshing. Int J Numer Meth Engng 1999;45:601–20.
[17] Moës N, Dolbow J, Belytschko T. A finite element method without remeshing. Int J Numer Meth Engng 1999;46:131–50.
[18] Moës N, Gravouil A, Belytschko T. Non planar 3d crack growth by the extended finite element and level sets – Part I: Mechanical model. Int J Numer Meth Engng 2002;53:2549–68.
[19] Gravouil A, Moës N, Belytschko T. Non planar 3d crack growth by the extended finite element and level sets – Part II: Level set update. Int J Numer Meth Engng 2002;53:2569–86.
[20] Réthoré J, Gravouil A, Combescure A. An energy conserving scheme for dynamic crack growth with the extended finite element method. Int J Numer Meth Engng 2005;63:631–59.
[21] Prabel B, Combescure A, Gravouil A, Marie S. Level set non-matching meshes: application to dynamic crack propagation in elastic-plastic media. Int J Numer Meth Engng 2007;69:1553–69.
[22] Reytier M, Chapuliot S, Marie S, Nédélec M. Thermomechanical analysis of thermal shock fracture in the brittle/ductile transition zone – Part II: Numerical calculations and interpretation of the test results. Engng Fract Mech 2006;73:283–95.
[23] Reytier M, Chapuliot S, Marie S, Ferry L, Nédélec M. Study of cleavage initiation under thermal shock by tests on cracked rings and thermomechanical calculations. Nucl Engng Des 2006;236:1039–50.
[24] Cast3M. Finite element software developed by the CEA (French atomic energy commission). <http://www-cast3m.cea.fr/>; 2007.
[25] Chapuliot S, Marie S, Dubarle PE. Première campagne de caractérisation de l'acier 16MND5 des essais FISTER. CEA, Rapport SEMT/LISN/00 -001/A; 2001.
[26] Chapuliot S, Lacire MH, Marie S, Nédélec M. Thermomechanical analysis of thermal shock fracture in the brittle/ductile transition zone – Part I: Description of the tests. Engng Fract Mech 2005;72:661–73.
[27] Tanguy B. Modélisation de l'essai Charpy par l'approche locale de la rupture: Application au cas de l'acier 16MND5 dans le domaine de transition. PhD thesis, Ecole des Mines de Paris; 2001.

[28] Rossoll A. Local approach of ductile cast iron fracture toughness measured by Charpy test. PhD thesis, Centrale Paris – TVFA TU Wien; 1993.
[29] Cowper GR, Symonds PS. Strain-hardening and strain-rate effects in the impact loading of cantilever beams. Division of Applied Mathematics, Brown University; 1957.
[30] Zhao H, Gary G. On the use of SHPB techniques to determine the dynamic behavior of materials in the range of small strains. Int J Solids Struct 1996;33:3363–75.
[31] American Society for Testing and Material. A2 – special requirements for testing compact specimen. ASTM E1820, US ASTM; 1986.
[32] Bryan RH, Bass BR, Merkle JG. The heavy-section steel technology pressurized-thermal-shock experiment, PTSE-1. Engng Fract Mech 1986;23:81–97.
[33] Genty A. Etude expérimentale et numérique de l'amorçage et de l'arrêt de fissure sous choc thermique dans un acier faiblement allié (16MND5). PhD thesis, Ecole des Mines de Paris; 1989.
[34] Iung T, Pineau A. Dynamic crack propagation and crack arrest investigated with a new specimen geometry: Part I: Experimental and numerical calculations. Fatigue Fract Engng Mater Struct 1996;19:1357–67.
[35] Iung T, Pineau A. Dynamic crack propagation and crack arrest investigated with a new specimen geometry: Part II: Experimental study on a low-alloy ferritic steel. Fatigue Fract Engng Mater Struct 1996;19:1369–81.
[36] Kanninen MF, Popelar C, Gehlen PC. Dynamic analysis of crack propagation and arrest in the double-cantilever-beam specimen. ASTM Special Technical Publication; 1977. p. 19–38.
[37] Seelig T, Gross D, Pothmann K. Numerical simulation of a mixed-mode dynamic fracture experiment. Intl J Fract 1999;99:325–38.
[38] Belytschko T, Krongauz Y, Organ D, Fleming M, Krysl P. Meshless methods: an overview and recent devleopments. Comp Meth Appl Mech Engng 1996;139:3–47.
[39] Jirasek M, Zimmerman T. Embedded crack model: I basic formulation. Int J Numer Meth Engng 2001;50:1269–90.
[40] Babuska I, Melenk JM. The partition of unity method. Int J Numer Meth Engng 1997;40:727–58.
[41] Duflot M. A study of the representation of cracks with level sets. Int J Numer Engng 2006;70:1261–302.
[42] Elguedj T, Gravouil A, Combescure A. Appropriate extended functions for XFEM simulation of plastic fracture mechanics. Comp Meth Appl Mech Engng 2006;195:501–15.
[43] Wyart E, Coulon D, Duflot M, Pardoen T, Remacle JF, Lani F. A substructured FE-shell/XFE-3D method for crack analysis in thin-walled structures. Int J Numer Meth Engng 2007;72:757–79.
[44] Chevaugeon N, Moës N, Minnebo H, Bechet E. Robust computation of stress intensity factor within the extended finite element context. In: International conference on computational fracture and failure of materials and structures, CFRAC 2007, Nantes, France; 2007.
[45] Newmark NM. A method of computation for structural dynamics. Proc ASCE 1959;85:67–94.
[46] Ortiz M, Simo JC. An analysis of a new class of algorithms for elastoplastic constitutive relations. Int J Numer Meth Engng 1986;23:353–66.
[47] Rice JR. A path independant integral and the approximate analysis of strain concentration by notches and cracks. Division of Engineering, Brown University; 1967.
[48] Nguyen TD, Govindjee S, Klein PA, Gao H. A material force for inelastic fracture mechanics. J Mech Phys Solids 2005;53:91–121.
[49] Mataga PA, Freund LB, Hutchinson JW. Crack tip plasticity in dynamic fracture. J Phys Chem Solids 1987;48:985–1005.
[50] Xu Y, Saigal S. An element free Galerkin analysis of steady dynamic growth of a mode I crack in elastic plastic materials. Int J Solids Struct 1999;36:1045–79.
[51] Mariani S, Perego U. Extended finite element method for quasi-brittle fracture. Int J Numer Meth Engng 2003;58:103–26.
[52] Wells GN, Sluys LJ. A new method for modelling cohesive cracks using finite elements. Int J Numer Meth Engng 2001;50:2667–82.
[53] Remmers JC, De Borst R, Needleman A. The cohesive segment method for the simulation of dynamic fracture. IUTAM symposium on discretization methods for evolving discontinuities, Lyon, France; 2006.
[54] Hahn GT, Hoagland RG, Kanninen MF, Rosenfield AR. Crack arrest in steels. Engng Fract Mech 1975;7:583–91.
[55] Kobayashi AS, Seo K, Jou JY, Urabe Y. A dynamic analysis of modified compact-tension specimens using homalite-100 and polycarbonate plates. Exp Mech 1980;20:73–9.
[56] Erdogan F, Sih GC. On the crack extension in plates under plane loading and transverse shear. J Basic Engng 1963;85:519–27.
[57] Oliver J, Huespe AE. Theoretical and computational issues in modelling material failure in strong discontinuity scenarios. Comp Meth Appl Mech Engng 2004;193:2987–3014.
[58] Oliver J, Huespe AE. Continuum approach to material failure in strong discontinuity settings. Comp Meth Appl Mech Engng 2004;193:30–2.
[59] Dumstorff P, Meschke G. Crack propagation criteria in the framework of X-FEM-based structural analyses. Int J Numer Anal Meth Geomech 2007;31:239–59.